

# Resistance Recognition of Moving Guidewire in Vascular Interventional Operation

Chuqiao Lyu<sup>1</sup>, Shuxiang Guo<sup>1,2\*</sup>, Youchun Ma<sup>1</sup>, Yue Wang<sup>1</sup>, Chenguang Yang<sup>1</sup>

<sup>1</sup> Key Laboratory of Convergence Biomedical Engineering System and Healthcare Technology, The Ministry of Industry and Information Technology, School of Life Science, Beijing Institute of Technology, No.5, Zhongguancun South Street, Haidian District, Beijing 100081, China

<sup>2</sup> Faculty of Engineering, Kagawa University, 2217-20 Hayashi-cho, Takamatsu, Kagawa 760-8521, Japan

E-mails: { guoshuxiang & lyuchuqiao }@bit.edu.cn;

\* Corresponding author

**Abstract** – Vascular interventional surgery is prevalent in treating cardiovascular and cerebrovascular diseases because of its low-invasive and rapid recovery. Surgeons cannot observe the vascular contour in real-time during the operation. So it is a technical task. In this paper, we try to research the problem by using the object detection and recognition model. We divide the guidewire moving in the 2D image into two states: resistance deformation and non-resistance deformation. Then we use the Faster-RCNN to classify and track the guidewires in phantom and synthetic surgical videos. The operation datasets in the phantom come from the PCI trainer. After extracting the mask of the guidewire as the ground truth, we randomly add the factual X-ray image information of the patient in the background. Finally, we compare the recognition results of the two cases. The model converges on the validation datasets, which proves that our method is effective. In vascular interventional surgery, the AI model can learn the expert experience, which may render an idea for the development of surgical robots.

**Index Terms** – Vascular interventional surgery, Faster RCNN, Resistance movement.

## I. INTRODUCTION

Because of low-invasive and rapid recovery advantages, vascular interventional surgery is prevalent in treating cardiovascular and cerebrovascular diseases. During the operation, the surgeon used X-ray equipment to observe the procedure. The long-term process will cause irreversible damage to the surgeon's body. The vascular interventional robot can avoid the surgeon's radiation exposure through the master-slave control mode [1],[2]. After several years of development, robot structure has gradually become an important research field [3]-[5]. In addition to specific control modules, environment perception modules can also help surgeons find the risks in time. For instance, they use robots to control the catheters or guidewires with low resistance through force feedback [6]-[8]. Some researchers use ultrasound equipment to supplement the depth

information and help doctors to locate the equipment accurately. The essence of these methods is to assist surgeons in operating catheters or guidewires to the target position smoothly. The operation skill given by robots to surgeons is a critical direction [9]-[12].

In recent years, the rapid development of deep learning has greatly enhanced the visual perception of robots. For example, the image segmentation based on U-net [13] can learn the surgeon's annotation and automatically segment computed tomography (CT) lung lesions. The YOLOv3 [14] algorithm can identify the end of the guidewire in real-time, which is helpful to improve the visual perception of surgical robots. In the general vascular intervention procedure, the master-slave robot can keep the operator away from the operating table. However, the assistants must stay in the operating room to monitor the robot operation to avoid risk. Some researchers proposed identifying force fluctuation through the CNN model, judging the current operation risk, and guiding doctors to operate [15]. When the force exceeds the warning line, the risk is already occurring. In more cases, surgeons can judge the risk by observing the low-resolution x-ray video, and the main feature that affects the surgeons' judgment is the shape of guidewires or catheters. Most of the time, the vascular contour is invisible. Experienced surgeons will judge the current operational risk according to the characteristics of angiographic and shapes. Some researchers try to help surgeons improve operation skills through virtual reality system [16]. Some researchers have tried to segment the moving guidewire in vascular. The results show that bone or residual contrast agents will affect the segmentation accuracy [17].

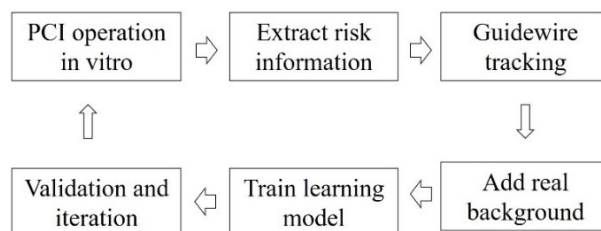


Fig. 1. The resistance motion recognition framework

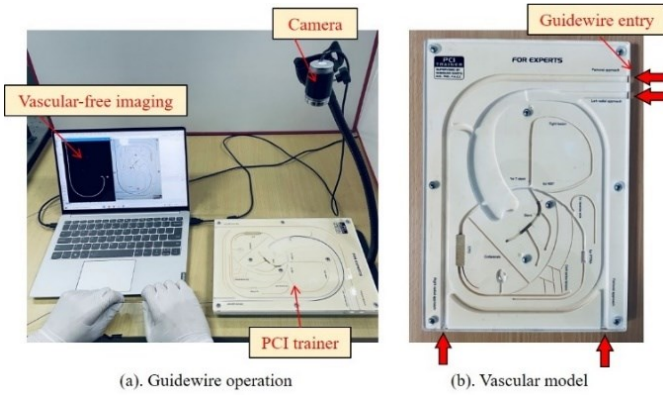


Fig. 2. PCI training platform for vascular interventional surgery

In this paper, we summarized the following deficiencies exist in the visual perception of the vascular interventional surgery robot:

- 1) The robot cannot accurately identify the guidewire or catheter, that is hard to judge the operation risk according to the x-ray image.
- 2) It is challenging to extract expert experience in surgery. Moreover, the surgical risk is not easy to define, and it is hard to establish adequate datasets.

## II. SYSTEM COMPOSITION

For problem A, this paper attempts to establish a guidewire identification and risk assessment model in non-vascular visual states using Faster-RCNN. This deep learning model can track the guidewire motion in real-time. To solve problem B, we try to collect datasets in the PCI trainer model in vitro, fill in the factual image through image processing algorithms, and construct guidewire tracking and risk identification datasets. The overall frame is shown in Fig. 1.

With the PCI trainer model in vitro, we can judge the operation risk more accurately. Because the PCI vascular model is 2D, the camera can capture RGB images like X-ray. If we collect 3D images with RGB images, the refraction of water flow will cause guidewire distortion. After collecting the PCI trainer operation, we can mark the abnormal bending and collision of the guidewire tip. This process is regarded as a gold standard when the vascular is visible. The phantom datasets are manually labelled as risk or non-risk. The way is to find the resistance deformation on the moving guidewire tip. We train a faster-RCNN algorithm to track such risks. In order to build a non-vascular environment, we find the open-source chest X-ray datasets. We extract masks from the guidewire and randomly placed them in any position of X-ray to build a counterfeit dataset. In the last part, we discuss the verification results of the model and give the conclusion.

## III. EXPERIMENTAL METHODS

### A. PCI data acquisition in vitro.

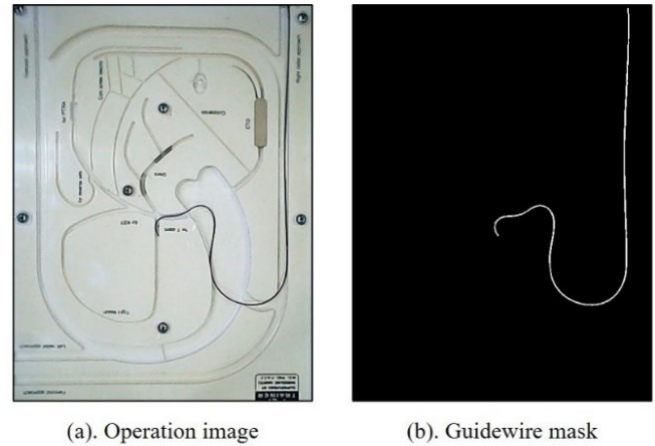


Fig. 3. Guidewire motion state extraction.

We use a vascular phantom (PCI Trainer for Experts, Medialpha Co., Ltd.) to collect guidewire operation videos. PCI trainer is a 2D training model for interventional surgeons, which contains many PCI operations. For example, stent, chronic total occlusion (CTO), etc. We used a standard guidewire (J-shape) to simulate PCI operation in the model. As shown in Fig. 2, the platform includes a camera, PCI trainer, guidewire, and operation interface. The size of the collected image is  $640 \times 480$ . We get the image only containing the guidewire mask by image subtraction, which superimposes the factual image background. In PCI trainers, the coarsest vascular is the aortic arch, about  $10mm$ . The thinnest vascular is  $1mm$ . We almost insert guidewires into all positions of the PCI trainer to collect images of the guidewire deformation. Finally, we collected a total of  $25min$  videos,  $20Hz$ ,  $30000$  images as metadata. We segment the moving guidewire, as shown in Fig. 3. Firstly, we use the empty PCI model for image subtraction, add a gaussian smoothing filter to filter the noise, and get a clearer guidewire deformation mask.

### B. Marking the resistance of moving guidewire.

In the process of intervention, the most critical requirement is the resistance-free movement of the guidewire. It is the primary skill for surgeons to avoid danger. However, in the actual operation process, due to the material of the guidewire, the patient's vascular specificity, heart beating, and other factors, the contact force of the guidewire tip cannot be transmitted to the surgeon in real-time. Sometimes, the slight resistance deformation of the guidewire cannot be detected, which is easy to cause vascular rupture, thrombosis, and even increase the risk. Here we describe this situation through a schematic diagram, as shown in Figure 4.

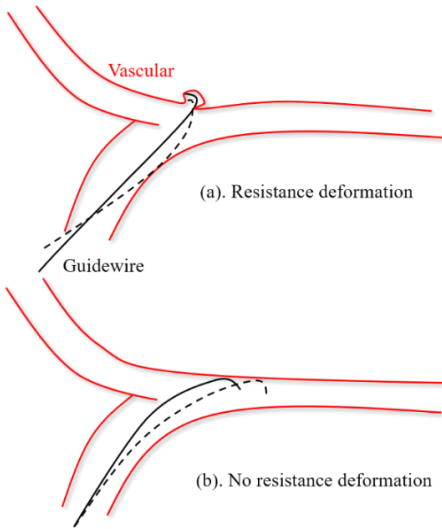


Fig 4. Resistance deformation diagram of guidewire.

As shown in Fig. 4, the guidewire is not easy to form a forward state with resistance, as shown in (a). Because of the remote intervention, the doctor's hand cannot sense the change of tip force. From the clinical experience, surgeons need to keep (b) state when operating guidewire to avoid the occurrence of a risk.

Therefore, the guidewire mask in the PCI trainer is labeled as resistance deformation and non-deformation frame by frame through manual annotation. Before labeling, we calculate the Hamming distance between images to determine whether the guidewire is moving. Before calculating the Hamming distance, we first calculate the hash value of the image. With judge the distance between the hash value of two frames, we can determine whether the guidewire is moving at this moment.

After determining the guidewire in motion, we cut the rectangular box of  $200 \times 300$  pixels around the moving guidewires as the first step to filter the mask datasets. We can further judge whether the guidewire is moving by the position change of the corners. The corner represents a pixel in the image. A small change in any direction will bring a significant change in the corner. The Shi-Tomasi corner analyzes the eigenvalue of the autocorrelation matrix  $M$ . If the smaller of the two eigenvalues are more significant than the minimum threshold, this pixel will be obtained as a strong corner. The Shi-Tomasi algorithm used in this paper is described as

$$E(u, v) \approx [u, v]M \begin{pmatrix} u \\ v \end{pmatrix}$$

$$M = \sum_{(x,y)} w(x, y) \begin{bmatrix} I_x^2 & I_x I_y \\ I_x I_y & I_y^2 \end{bmatrix} \rightarrow R^{-1} \begin{bmatrix} \lambda_1 & 0 \\ 0 & \lambda_2 \end{bmatrix} R$$

$$ST_R = \min(\lambda_1, \lambda_2) \quad (1)$$

Where  $E$  represents the change of gray value when the window moves in all directions,  $I_x$  and  $I_y$  are the gradients in  $X$  and  $Y$  directions, and  $u$  and  $v$  represent the displacement of the moving window.  $R$  represents the rotation factor. It does not affect the variation component. Shi-Tomasi algorithm determines whether the current point is a corner by judging the minimum eigenvalue of matrix  $M$ .

In this way, we get the bounding boxes of guidewires and the categories of resistance states. Finally, we get 2792 mask images with labels from the 25min operation video. The image with wrong mask segmentation is eliminated. The masked guidewire statistics are shown in Table I.

Table I

The masked guidewire datasets statistics

State	Static	Moving		Others
		Resistance	Non-resistance	
Frames	1676	596	519	207
Percentage	55.88%	19.89%	17.30%	6.92%

Table II

The training datasets statistics

Type	Training		Testing	
	Resistance	Non-resistance	Resistance	Non-resistance
Number	22760	20760	5690	5190
Rotation	(0°, 90°, 180°, 270°)		(0°)	
Chest X-ray	40		10	

### C. Training datasets preprocessing

The actual X-ray background is very complex. In order to simulate the natural operation environment, we choose the NIH ChestX-ray14 [18] as the background of the guidewire mask. As shown in Fig. 5, ChestX-ray14 mainly comes from patients with 14 kinds of lung diseases. It has 112120 front views of 30805 patients. Here we only select 50 healthy samples as the background. The guidewire with bounding box moves at any position of X-ray. We randomly place the guidewire mask in the red dotted line, covering the joint positions in PCI operation, as shown in Fig. 5(c). At the same time, we also rotate the training images randomly, so the dataset is expanded four times. Here, the image resolution

from the ChestX-ray14 is  $1024 \times 1024$ . Two images' pixels are covered one by one. Then we divide the pseudo-X-ray image into  $500 \times 500$  randomly. The principle of segmentation is that each image must contain the outline of a guidewire. We also separate the data in the form of 8:2 for model training and testing. There is only one guidewire mask in each X-ray. In model validation, we always choose the most interesting bounding box as the classification target. The final statistics of training data are shown in Table II.

#### D. Fast RCNN model training

Considering that the actual X-ray image is of high resolution, this paper selects fast RCNN as the training model of guidewire tracking and resistance detection. Fast RCNN consists of four parts.

- 1) Convolution layers. As a CNN network target detection method, Faster RCNN extracts feature maps of an image through the convolution layer.
- 2) Region proposal networks (RPN). RPN generates region proposals. In this layer, we use Softmax to judge whether the anchors are positive or negative, and then we use the bounding box region to modify the anchors to obtain accurate propositions.
- 3) ROI pooling. This step integrates the input feature maps and region proposals of the previous layer, extracts the proposal feature maps after synthesizing this information, and sends them to the subsequent connection layer to determine the target category.
- 4) Fully connected layer. The category of proposals is calculated by proposal feature maps, and the final accurate position of the detection box is obtained by bounding box region again.

Different from the fast RCNN used in this paper, our final FCN is used for binary classification. The classification loss use cross-entropy, and the bounding box regression use smooth-l. SDG optimizes the model. The loss of both is shown in the following:

$$L_{cls}(p_i, p_i^*) = - \sum_i p_i^* \log(p_i) \quad (3)$$

$$L_{reg}(t_i, t_i^*) = \sum_{i \in x, y, w, h} smooth_{L1}(t_i - t_i^*)$$

$$smooth_{L1}(x) = \begin{cases} 0.5x^2 & \text{if } |x| < 1 \\ |x| - 0.5 & \text{otherwise} \end{cases} \quad (4)$$

Where  $i$  represents the anchors index.  $p_i$  represents the positive Softmax probability.  $p_i^*$  represents the ground truth predict probability.  $t_i$  represents the predict bounding box and  $t_i^*$  represents the ground truth box. Other hyperparameters used in the model are shown in Table III.

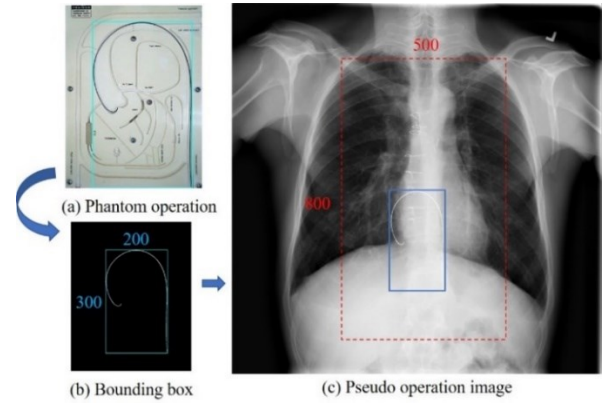


Fig 5. Operation image compose.

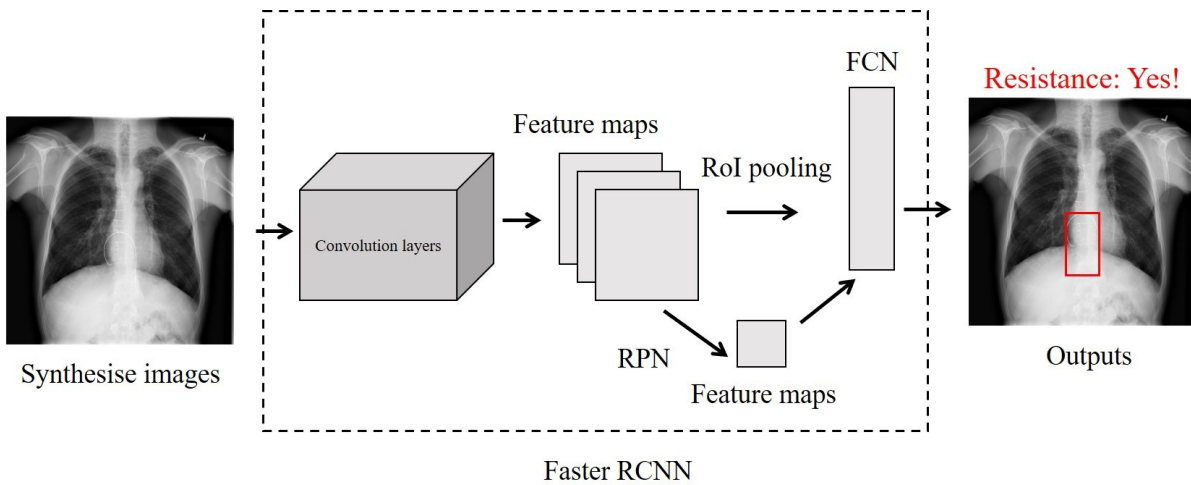


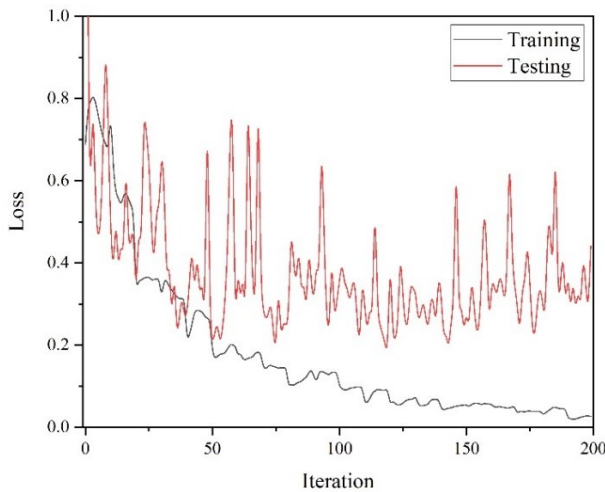
Fig. 6. Guidewire tracking and resistance identification based on Faster RCNN

#### IV. RESULTS AND DISCUSSION

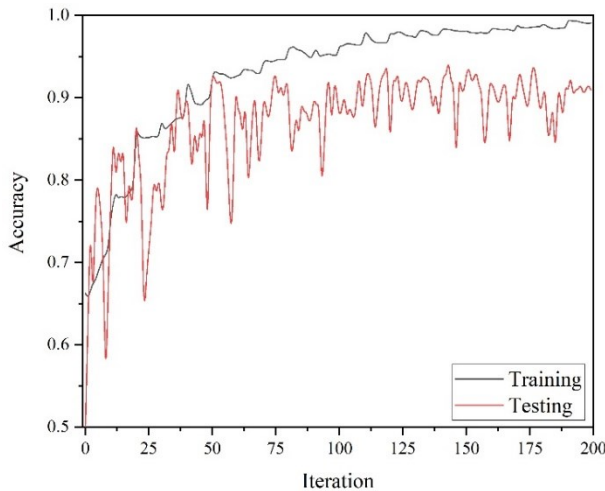
Tabel III

The training hyper-parameters

Hyper-parameters	Value
epochs	20
batch size	1
learning rate	0.001
learning decay	1e-5
decay gamma	0.1



(a). The binary classification losses



(b). The binary classification accuracies

Fig. 7. The training results of Faster RCNN

Faster RCNN usually use the pre-trained CNN model. Here we choose Resnet-18 in C2L as the pre-training feature model [19] in this paper. C2l is a pre-training method based on an extensive range of 2D radiographs only. We use Anaconda 3, Python 3.8, Pytorch 1.7.1, Cuda 11.1 and Cudann 9.1 as the training environment. Firstly, we train the RPN network, in which the classification IoU of anchors is between 0.3 and 0.7, then we collect proposals through the trained RPN network. Finally, we train the whole Faster RCNN. The loss function of the whole network is as follows:

$$L(p_i, t_i) = \frac{1}{N_{cls}} \sum_i L_{cls}(p_i, p_i^*) + \lambda \frac{1}{N_{reg}} \sum_i p_i^* L_{reg}(t_i, t_i^*) \quad (5)$$

Where  $\lambda$  is used to balance two training losses. We choose 0.5 in this paper.

We calculate the training results of the fast RCNN model based on C2L pre-training in 20 epochs. Each epoch represents a complete cycle, and we record 10 iterations for each epoch. The results of model training and validation are shown in Fig. 7. From Fig. 7, we can see that the model converges at the 50th iteration, but the test accuracy and loss continue to fluctuate. It may be related to the imbalance of data distribution between the training sets and testing sets. If we increase the diversity of phantom and guidewire masks, the problem can be solved. After 50 iterations, the average testing accuracy of Faster RCNN model is 86.54%. Other results are shown in Table IV.

Table IV

The model testing results

Results	Recall	Precision	F1
Non-resistance	0.9672	0.8027	0.8773
Resistance	0.7648	0.9593	0.8511

The results show that the sample recall value of non-resistance motion is 96.72%, and the precision of resistance motion is 95.93%, which proves that the model can better distinguish the non-resistance motion of guidewire. However, the precision value of non-resistance motion is 80.27%, and the recall value of resistance motion is 76.48%, which indicates that the model is easy to misjudge the resistance samples as non-resistance samples. It may be due to the error of annotation. In the video, the deformation of the guidewire in the non-resistance motion may be small, which makes the model misjudge.

## V. CONCLUSION

In this paper, we try to build a vision-based guidewire video algorithm model in a non-vascular environment. We use the phantom platform to collect guidewire motions and use the Shi-Tomasi algorithm and Hamming distance to filter the duplicate images. Then, through manual labeling, we divide the moving guidewire into resistance state and non-resistance state and obtain the guidewire mask. Next, we access the public dataset s ChestX-ray14 to obtain the actual patient's X-ray chest images as the background information, and we also add the guidewire to the X-ray according to a certain proportion to get the bounding box. We get the Resnet18 pre-training model based on extensive X-ray datasets from C2L as the feature network of Faster RCNN. Finally, we train the whole network, and the training results show that the resistance recognition model can give a good precision, which is 95.93%, but recall is only 76.48%. We analyze that the resistance deformation of the guidewire is too small to make the model misjudge. Finally, our method provides a good idea for combining expert experience and AI algorithm in vascular interventional surgery. Unlike force feedback [20], it has reference value for the related research of expanding the visual perception function of vascular interventional surgery robots.

## ACKNOWLEDGMENT

This work was supported in part by the National Natural Science Foundation of China (61703305), in part by National High-tech Research and Development Program (863 Program) of China (2015AA043202), in part by SPS KAKENHI (15K2120) in part by Key Research Program of the Natural Science Foundation of Tianjin (18JCZDJC38500), and in part by Innovative Cooperation Project of Tianjin Scientific and Technological Support (18PTZWHZ00090).

## REFERENCES

- [1]. X. Bao et al., "Operation evaluation in-human of a novel Remote-controlled vascular interventional robot," *Biomedical Microdevices*, vol.20, no.2, 2018, doi:10.1007/s10544-018-0277-5.
- [2]. X. Bao et al., "Compensatory force measurement and multimodal force feedback for remote-controlled vascular interventional robot," *Biomedical Microdevices*, vol.20, no.3, 2018, doi:10.1007/s10544-018-0318-0.
- [3]. L. Zhang et al., "A Magnetorheological Fluids-based Robot-assisted Catheter/guidewire Surgery System for Endovascular Catheterization," *Micromachines*, vol.12, no.6, 2021, doi:10.3390/mi12060640.
- [4]. L. Zheng, S. Guo, "A Magnetorheological Fluid-based Tremor Reduction Method for Robot Assisted Catheter Operating System," *International Journal of Mechatronics and Automation*, vol.8, no.2, pp.72-79, 2021, doi:10.1504/IJMA.2021.115234.
- [5]. X. Bao et al., "Operation evaluation in-human of a novel Remote-controlled vascular interventional robot," *Biomedical Microdevices*, vol.20, no.2, 2018, doi:10.1007/s10544-018-0277-5.

- [6]. J. Guo, X. Jin, S. Guo and Q. Fu, "A Vascular Interventional Surgical Robotic System Based on Force-Visual Feedback," *IEEE Sensors Journal*, vol. 19, no. 23, pp. 11081-11089, 1 Dec.1, 2019, doi:10.1109/JSEN.2019.2935002.
- [7]. X. Jin et al., "Development of a Tactile Sensing Robot-Assisted System for Vascular Interventional Surgery," *IEEE Sensors Journal*, vol. 21, no. 10, pp. 12284-12294, 15 May15, 2021, doi:10.1109/JSEN.2021.3066424.
- [8]. S. Guo et al., "A Novel Robot-Assisted Endovascular Catheterization System with Haptic Force Feedback," *IEEE Transactions on Robotics*, vol.35, no.3, pp.685-696, 2019, doi:10.1109/TRO.2019.2896763.
- [9]. S. Guo et al., "Machine learning-based Operation Skills Assessment with Vascular Difficulty Index for Vascular Intervention Surgery," *Medical & Biological Engineering & Computing*, vol.58, no.8, pp.1707-1721, 2020, doi:10.1007/s11517-020-02195-9.
- [10]. Y. Zhao et al., "A novel noncontact detection method of surgeon's operation for a master-slave endovascular surgery robot," *Medical & Biological Engineering & Computing*, vol.58, no.4, pp.871-885, 2020, doi:10.1007/s11517-020-02143-7.
- [11]. S. Guo et al., "A Surgeon's Operating Skills-based Non-interference Operation Detection Method for Novel Vascular Interventional Surgery Robot Systems," *IEEE Sensors Journal*, vol.20, no.7, pp.3879-3891, 2019, doi:10.1109/JSEN.2019.2960926.
- [12]. C. Yang et al., "A Vascular Interventional Surgical Robot Based on Surgeon's Operating Skills," *Medical & Biological Engineering & Computing*, vol.57, no.9, pp.1999-2010, 2019, doi:10.1007/s11517-019-02016-8.
- [13]. Gaál G, Maga B, Lukács A, "Attention u-net based adversarial architectures for chest x-ray lung segmentation," *arXiv preprint*, 2020, arXiv:2003.10304.
- [14]. R. -Q. Li et al., "Real-Time Multi-Guidewire Endpoint Localization in Fluoroscopy Images," *IEEE Transactions on Medical Imaging*, doi:10.1109/TMI.2021.3069998.
- [15]. Y. Zhao et al., "A CNN-based prototype method of unstructured surgical state perception and navigation for an endovascular surgery robot," *Med Biol Eng Comput*, vol. 57, pp. 1875-1887, 2019, doi:10.1007/s11517-019-02002-0.
- [16]. S. Guo, X. Cai, B. Gao, "A Tensor-Mass Method-based Vascular Model and its Performance Evaluation for Interventional Surgery Virtual Reality Simulator," *The International Journal of Medical Robotics and Computer Assisted Surgery*, vol.14, no.6, 2018, doi:10.1002/rcs.1946.
- [17]. Nguyen, Anh, et al., "End-to-End Real-time Catheter Segmentation with Optical Flow-Guided Warping during Endovascular Intervention." *2020 IEEE International Conference on Robotics and Automation (ICRA)*, 2020, pp. 9967-9973, doi: 10.1109/ICRA40945.2020.9197307.
- [18]. P. Rajpurkar et al., "Chexnet: Radiologist-level pneumonia detection on chest x-rays with deep learning," *arXiv preprint*, 2017, arXiv:1711.05225.
- [19]. H.Y. Zhou et al, "Comparing to Learn: Surpassing ImageNet Pretraining on Radiographs by Comparing Image Representations," *Medical Image Computing and Computer Assisted Intervention - MICCAI 2020. Lecture Notes in Computer Science*, vol. 12261, 2020, doi:10.1007/978-3-030-59710-8\_39.
- [20]. Y. Song, "Performance evaluation of a robot-assisted catheter operating system with haptic feedback," *Biomedical Microdevices*, vol.20, no.2, 2018, doi:10.1007/s10544-018-0294-4.